

# Design and analysis of redshift surveys

A.F. Heavens and A.N. Taylor

*Institute for Astronomy, University of Edinburgh, Royal Observatory, Blackford Hill, Edinburgh, U.K.*

14 March 2021

## ABSTRACT

In this paper we consider methods of analysis and optimal design of redshift surveys. In the first part, we develop a formalism for analysing galaxy redshift surveys which are essentially two-dimensional, such as thin declination slices. The formalism is a power spectrum method, using spherical coordinates, allowing the distorting effects of galaxy peculiar velocities to be calculated to linear order on the assumption of statistical isotropy but without further approximation. In this paper, we calculate the measured two-dimensional power for a constant declination strip, widely used in redshift surveys. We present a likelihood method for estimating the three-dimensional real-space power spectrum and the redshift distortion simultaneously, and show that for thin surveys of reasonable depth, the large-scale 3D power cannot be measured with high accuracy. The redshift distortion may be estimated successfully, and with higher accuracy if the 3D power spectrum can be measured independently, for example from a large-scale sky-projected catalogue.

In the second part, we show how a 3D survey design can be optimized to measure the power spectrum, considering whether areal coverage is more important than depth, and whether the survey should be sampled sparsely or not. We show quite generally that width is better than depth, and show how the optimal sparse-sampling fraction  $f$  depends on the power  $P$  to be measured. For a Schechter luminosity function, a simple optimization  $fP \simeq 500h^{-3} \text{ Mpc}^3$  is found.

## 1 INTRODUCTION

The measurement of fluctuation power in the galaxy distribution is an important test of galaxy formation models, since the fluctuation spectrum, of mass at least, is predicted readily by such models. Power can be measured from three-dimensional redshift surveys, or from projected catalogues, by numerical inversion techniques. Redshift surveys have the advantage (and disadvantage) that they are distorted by the effects of peculiar velocities, and can therefore be used to extract information on the density parameter, under the assumption that structure grows by gravitational instability. One has then the possibility of measuring three-dimensional power and the density parameter (via  $\beta \equiv \Omega_0^{0.6}/b$ , where  $b$  is the bias parameter for the survey in hand) from a galaxy redshift survey (Heavens & Taylor 1995; hereafter HT95; see also Kaiser 1987, Hamilton 1992, Cole et al. 1994).

It is clear that the longest wavelength which can be measured is limited by the size of the survey, so it is attractive to consider surveys which are essentially one- or two-dimensional, to maximise at least one dimension without incurring prohibitive cost in observation time (e.g. Broadhurst et al 1990). The difficulty with such an approach as a method for measuring the power spectrum is that a low-dimensional power measurement at a given wavenumber will have a contribution (which may be dominant) from much smaller scales in three dimensions (e.g. Kaiser & Peacock 1991). The interpretation of the observed power spectrum can therefore be difficult. For surveys which do not correspond to the ‘distant-observer’ approximation (cf. Kaiser

1987), the power spectrum measurement and the redshift distortion become linked, and this further complicates the analysis.

The ease with which the parameters of interest may be extracted depends on the choice of coordinate system and basis functions in which the density field is expanded. For two reasons the choice of spherical polar coordinates is compelling. Firstly the survey is almost certain to be defined in terms of a fixed areal coverage (independent of depth), and secondly, a flux limited survey will have a selection function  $\phi$  (or, equivalently, a mean observed density  $\rho_0(r)$ ) which is dependent on distance, but not on direction. The mean density of the survey is then separable in spherical coordinates  $\bar{\rho}(\mathbf{r}) = \rho_0(r)M(\theta, \varphi)$ , where  $M$  is either 1 or 0 depending on whether the direction  $(\theta, \varphi)$  is in the survey or not. The second reason is that, unless  $\beta \ll 1$ , it is impossible to ignore redshift distortion effects, and since the distortion between the real-space map and the redshift-space map is purely radial, it is straightforward to include the distortion in a power-spectrum analysis in spherical coordinates (cf. Zaroubi & Hoffman 1996).

The choice of basis functions must also be done with some care. It is very useful to choose functions which pick up a narrow range of wavenumbers from three-dimensional space. In this regard, spherical Bessel functions are ideal, and they also have advantages in that the redshift distortion is relatively simple in this system. An arbitrary choice of functions (or equivalently, an arbitrary choice of projection onto the sky) makes the interpretation of measured 2D

arXiv:astro-ph/9705215v1 27 May 1997

power difficult, since the 3D wavenumbers contributing to the power may be poorly constrained. Even in this idealized case, the range of 3D power contributing to the 2D coefficients can be large, especially for thin surveys of a few degrees thickness. In these cases, 3D power spectrum at large scales becomes difficult to achieve with high accuracy.

One of the aims of the paper up to this point is to demonstrate that the expected accuracy of a proposed survey in measuring some parameter can be estimated in advance, and this sort of study can and should influence how a survey is designed, whether in 2D or 3D. We investigate in section 4 how 3D design may be optimised for power spectrum estimation, subject to constraints. We find that, if observing time is constrained, then it is always better to cover a large area on the sky, rather than going deep. In some cases it can be advantageous to sample galaxies sparsely, with the sparse-sample fraction being dependent on the power to be measured and the luminosity function of the galaxies. We present a very simple formula for calculating the optimal sparse-sample fraction.

The paper is laid out as follows: in Section 2 we consider power measurements in idealised cases of 1D and 2D surveys, which highlight the problems which such surveys have to address. In Section 3 we present a new method for analysing constant declination strips, for measuring the real-space power spectrum and redshift distortion. In Section 5, we solve the problem of designing surveys optimised for 3D power estimation.

## 2 1D AND 2D: GENERAL CONSIDERATIONS

The fractional overdensity is  $\delta(\mathbf{r}) \equiv \rho(\mathbf{r})/\bar{\rho} - 1$ , where  $\bar{\rho}$  is the mean density. Our Fourier transform convention is  $\delta_{\mathbf{k}} \equiv \int d^3\mathbf{r} \delta(\mathbf{r}) e^{-i\mathbf{k}\cdot\mathbf{r}}$  with inverse  $\delta(\mathbf{r}) \equiv \frac{1}{(2\pi)^3} \int d^3\mathbf{k} \delta_{\mathbf{k}} e^{i\mathbf{k}\cdot\mathbf{r}}$ . The Power spectrum is defined by

$$\langle \delta_{\mathbf{k}} \delta_{\mathbf{k}'}^* \rangle \equiv (2\pi)^3 P_{3D}(k) \delta^D(\mathbf{k} - \mathbf{k}') \quad (1)$$

so that the correlation function is

$$\xi(r) = \frac{1}{(2\pi)^3} \int d^3\mathbf{k} P_{3D}(k) e^{i\mathbf{k}\cdot\mathbf{r}}. \quad (2)$$

In an idealized pencil-beam survey, the density field along a line is measured, and the 1D power spectrum estimated. To relate this to the 3D power spectrum, we follow Lumsden, Heavens & Peacock (1987), noting that the correlation function is the same along the line as in 3D, by isotropy.

$$\begin{aligned} P_{1D}(\bar{k}) &= \int dx \xi(x) \exp(-i\bar{k}x) \\ &= \frac{1}{(2\pi)^3} \int dx d^3\mathbf{k} P_{3D}(k) \exp(ik_x x) \exp(-i\bar{k}x) \end{aligned} \quad (3)$$

where we assume the pencil beam lies along  $y = z = 0$ . The integration over  $x$  gives a 1D delta function, and changing the remaining integration over  $k_x$  and  $k_y$  to a polar integration, we get

$$P_{1D}(k) = \frac{1}{(2\pi)^2} \int_{|k|}^{\infty} d\bar{k} P_{3D}(\bar{k}) \bar{k} \quad (4)$$

Hence we see that power in one dimension comes from *all* shorter wavelengths in 3D. This is readily understandable by

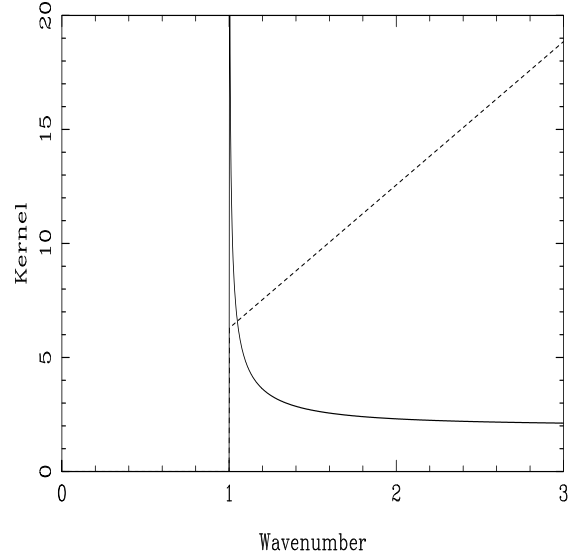


**Figure 1.** Kernel function  $G(k, \bar{k})/\bar{k}$  for a thin sheet (solid) and pencil-beam survey (dashed). The 2D wavenumber is unity.

consideration of the following 2D  $\rightarrow$  1D illustration: imagine looking along a corrugated roof at an angle to the corrugations. The separation of peaks along the line is longer in 1D by a geometrical factor, so the 1D power (averaged over angles) has contributions from 2D power at all shorter wavelengths.

Notice also that the 1D power spectrum must be a monotonically decreasing function of  $k$  (the squared amplitudes of the Fourier coefficients may not be monotonic, being drawn from a Rayleigh distribution). Also note that if the 3D power spectrum has a cutoff at some large wavelength, the 1D power spectrum will be constant (and non-zero) on all larger scales.

For comparison with later analysis in this paper, we define the kernel  $G(k, \bar{k})$  such that the measured power is

$$P(k) \equiv \int_0^{\infty} d \ln \bar{k} P_{3D}(\bar{k}) G(k, \bar{k}) \quad (5)$$

from which we see that the kernel for a 1D skewer is

$$G(k, \bar{k}) = 2\pi \bar{k}^2 \Theta(\bar{k} - k) \quad (6)$$

where  $\Theta$  is the Heaviside function. This unpleasant convolution function is shown in Figure 1 (throughout we plot  $G(k, \bar{k})/\bar{k}$ , since we use a linear rather than logarithmic  $k$  axis). For a practical pencil-beam survey, the kernel will be suppressed at high  $k$ , but this calculation illustrates the severe problems in interpreting the power spectrum of pencil-beam surveys – the 1D power may be coming from much larger wavenumbers in 3D.

For thin, infinite plane surveys, a similar analysis (Peacock 1991) gives

$$P_{2D}(k) = 2 \int_k^{\infty} d\bar{k} P_{3D}(\bar{k}) \frac{\bar{k}}{\sqrt{\bar{k}^2 - k^2}}. \quad (7)$$

The associated kernel  $G(k, \bar{k}) = 2\bar{k}^2 \Theta(\bar{k} - k) / \sqrt{k^2 - \bar{k}^2}$  is also shown in Figure 1. Again what one finds is that the kernel feeds a lot of power (if it exists) from high  $k$  to low  $k$ . If the plane survey is of finite thickness, the high- $k$  part of the kernel will be suppressed, and weighting of the data can help still further (see Section 3) but it is still possible that 2D power at  $k$  may have little connection with 3D power on such scales.

### 3 2D SURVEYS

For surveys which have one dimension considerably smaller than the other two, it is sensible to reduce the dimensionality of the survey by projection onto a 2D surface. We can then reduce the dimensionality of the transform correspondingly. As emphasized in the introduction, there are considerable advantages in using spherical coordinates for the analysis. The survey is almost certainly characterized by a radial selection function, and an angular selection defining the boundary (cf Fabbri & Natale 1990, Scharf et al. 1992, Scharf & Lahav 1993, Fisher et al 1994a,b 1995). Also, the effects of redshift distortion enter only in the radial direction. In the case of a thin slice survey, one avoids any difficulties which might be apparent in ‘flattening-out’ the survey into a plane suitable for cartesian analysis. One final point is that it is the largest scale modes where the radial nature of the distortion is most important to treat correctly.

In this section, we develop a 2D expansion of the density field projected onto a fixed declination, allowing for redshift distortions. We use coordinates  $s, \theta, \varphi$ , where  $s = cz/H_0$  is the distance assigned on the basis of the redshift  $z$ , assuming uniform expansion ( $H_0$  is the Hubble constant). This is the normal distance assigned in redshift surveys, and it differs from the true distance  $r$  because of peculiar velocities. In this paper we consider only  $z \ll 1$ , but the spherical coordinate system allow the effects of non-euclidean geometry and temporal evolution to be included if desired.

Our 2D expansion is based on the 3D Fourier-Bessel expansion of the density field (cf HT95, Lahav 1993):

$$\delta_{\ell m}(k) = \sqrt{\frac{2}{\pi}} \int d^3 \mathbf{r} \delta(\mathbf{r}) j_{\ell}(kr) Y_{\ell}^{m*}(\theta, \varphi) \quad (8)$$

with inverse

$$\delta(\mathbf{r}) = \sqrt{\frac{2}{\pi}} \sum_{\ell, m} \int dk k^2 \delta_{\ell m}(k) j_{\ell}(kr) Y_{\ell}^m(\theta, \varphi). \quad (9)$$

The statistical properties of  $\delta_{\ell m}(k)$  are derived in the appendix. We proceed by projecting all galaxies onto the central value  $\theta = \theta_0$ , and expand in terms of  $m$  and  $k$ . At this stage, we leave the choice of radial expansion function general,  $f(kr)$ . We also allow for radial and angular weighting of the data via the functions  $w_s(\mathbf{s})$  and  $w_{\Omega}(\Omega)$ , which may help in optimizing the signal-to-noise and apodizing. The radial weight may be  $k$ -dependent. For a constant declination strip, the obvious orientation of coordinates is to have the centre of the strip at constant  $\theta = \theta_0$ , and to expand in terms of  $m$ . We let the thickness be  $\Delta\theta$ , and the width  $\Delta\varphi$ , centred on  $\varphi = 0$ . Our choice of expansion is

$$\tilde{\rho}_m(k) \equiv \sqrt{\frac{2}{\pi}} \int d^3 \mathbf{s} \rho(\mathbf{s}) f(ks) \exp(-im\varphi) w_s(s) w_{\Omega}(\Omega). \quad (10)$$

As an important aside, there is an issue over which frame of reference should be used for redshift-space expansions of this sort. Should the redshift be measured in the Local Group frame or the Microwave Background frame? In either case, the redshift distance is

$$\mathbf{s}(\mathbf{r}) = \mathbf{r} \left[ 1 + \frac{(\mathbf{v} - \mathbf{v}_0) \cdot \mathbf{r}}{H_0 r^2} \right] \quad (11)$$

where  $\mathbf{v}_0$  is the peculiar velocity of the frame of reference. This relationship is general, but since we wish to make a perturbation expansion, we must ensure that the second term in the square brackets is always small. Assuming a sufficiently coherent velocity field such that  $\mathbf{v}$  approaches the Local Group velocity as  $r \rightarrow 0$ , we see that the expansion must be done in the Local Group frame.

The difference between the expansion coefficients and their mean values

$$\rho_m^0(k) = \sqrt{\frac{2}{\pi}} \int d^3 \mathbf{r} \rho_0(r) f(kr) \exp(-im\varphi) w_s(r) w_{\Omega}(\Omega) \quad (12)$$

can be related to the  $\delta_{\ell m}(k)$  by substituting for  $\delta(\mathbf{r})$  from (9), and noting that number conservation implies that  $\rho(\mathbf{r}) d^3 \mathbf{r} = \rho(\mathbf{s}) d^3 \mathbf{s}$ :

$$\begin{aligned} D_m(k) &\equiv \tilde{\rho}_m(k) - \rho_m^0(k) \\ &= \sum_{\bar{\ell}, \bar{m}} W_{\bar{\ell}}^{m\bar{m}} \int_0^{\infty} d\bar{k} \delta_{\bar{\ell}, \bar{m}}(\bar{k}) \Lambda_{\bar{\ell}}(k, \bar{k}) \bar{k}^2 \end{aligned} \quad (13)$$

where

$$\begin{aligned} W_{\bar{\ell}}^{m\bar{m}} &\equiv \sqrt{\frac{(2\bar{\ell} + 1)(\bar{\ell} - \bar{m})!}{4\pi(\bar{\ell} + \bar{m})!}} (-1)^{(\bar{m} + |\bar{m}|)/2} \times \\ &\frac{2 \sin[(\bar{m} - m)\Delta\varphi/2]}{(\bar{m} - m)} \int_{\cos(\theta_0 + \Delta\theta/2)}^{\cos(\theta_0 - \Delta\theta/2)} d\mu P_{\bar{\ell}}^{|\bar{m}|}(\mu) \end{aligned} \quad (14)$$

and

$$\begin{aligned} \Lambda_{\bar{\ell}}(k, \bar{k}) &= \Phi_{\bar{\ell}}(k, \bar{k}) + \beta V_{\bar{\ell}}(k, \bar{k}) \\ \Phi_{\bar{\ell}}(k, \bar{k}) &\equiv \frac{2}{\pi} \int_0^{\infty} dr \rho_0(r) j_{\bar{\ell}}(\bar{k}r) f(kr) w_s(r) r^2 \\ V_{\bar{\ell}}(k, \bar{k}) &\equiv \frac{2}{\pi \bar{k}^2} \int_0^{\infty} dr \rho_0(r) \frac{d}{dr} [f(kr) w_s(r)] \times \\ &\frac{d}{dr} [j_{\bar{\ell}}(\bar{k}r)] r^2. \end{aligned} \quad (15)$$

The signal part of the covariance matrix can be written as

$$\langle D_m(k) D_{m'}^*(k') \rangle \equiv \int d \ln \bar{k} P_{3D}(\bar{k}) G_{mm'}(k, k', \bar{k}) \quad (16)$$

where

$$G_{mm'}(k, k', \bar{k}) = (2\pi)^3 \sum_{\bar{\ell}} Z_{\bar{\ell}}^{mm'} \Lambda_{\bar{\ell}}(k, \bar{k}) \Lambda_{\bar{\ell}}(k', \bar{k}) \bar{k}^3 \quad (17)$$

and  $Z_{\bar{\ell}}^{mm'} \equiv \sum_{\bar{m}} W_{\bar{\ell}}^{m\bar{m}} W_{\bar{\ell}}^{m'\bar{m}*}$ . The shot noise contribution to the covariance matrix is

$$\begin{aligned} \langle D_m(k) D_{m'}^*(k') \rangle_{\text{SN}} &= \frac{2}{\pi} \int dr d\theta d\varphi \\ &r^2 \sin \theta \rho_0(\mathbf{r}) f(kr) f(k'r) \exp[i(m - m')\varphi] w_s^2(r) w_{\Omega}^2(\Omega). \end{aligned} \quad (18)$$

In practice, one splits  $D_m(k)$  into real and imaginary parts,

with similar, but more cumbersome, expressions for the covariance matrix elements. Some kernels are shown in Fig. 2 and 3 for a survey with a gaussian selection function  $\exp[-(r/r_*)^2]$ , with  $r_* = 450h^{-1}$  Mpc, with survey limits  $\Delta\theta = 6^\circ$  centred at declination  $30^\circ$ , and width  $\Delta\varphi = 90^\circ$ . The radial expansion function is chosen to be a spherical Bessel function, with  $\ell = 2$ . This choice is motivated in two ways. Firstly, we know that in 3D the Bessel functions give narrow kernels, so they seem a good start in 2D. A second, related point, is that the function gives little weight to the very nearby part of the survey. Since this is the thinnest part, it is likely to contribute significantly to aliasing difficulties. The weighting scheme chosen also helps in this regard. Fig. 3 shows kernels for plane waves with almost the same wavenumbers as Fig. 2, and with direction along the central  $\varphi$  value, to correspond as closely as possible to Fig. 2 (cf the analysis of the Las Campanas survey by Landy et al. 1996). These curves are simply integrals of the squared modulus of the window function transform, calculated via a  $200^3$  FFT, which accounts for their slightly ragged nature. The comparison between the methods is not quite straightforward, as the 2D modes look rather different. Note that the Fourier modes assume  $\beta = 0$ ; for non-zero  $\beta$ , the kernels are extremely complicated in the Fourier case. The comparison is most stark if one compares the dimensionality of the objects which one needs to calculate to include redshift distortions. In essence, the 2D coefficients are linear combinations of the 3D coefficients. If no simplification is possible, one needs to calculate a 5D object to calculate a range of 2D coefficients. This is required if one uses Fourier modes (Zaroubi & Hoffman 1996, equation 10), but using the spherical modes reduces the dimensionality such that the most complicated objects are only 3D (see (13)). It is this fact that the kernels for non-zero  $\beta$  can be readily calculated for the spherical modes which is their major advantage. It arises, of course, from the radial nature of the distortion and selection function, and the use of angular coordinates to delimit the survey.

For high  $m$  the spherical kernels are sometimes not centred on  $k$ , and the 2D power may come principally from shorter wavelengths in 3D. The effects of this, and shot noise and cosmic variance can be accounted for correctly using likelihood techniques, so the 3D power spectrum can be estimated, but it is clear from Figs. 2 and 3 that the task is not going to be easy, whichever method is used. The accuracy with which the power and  $\beta$  determination can be done with the Fourier-Bessel transform is explored in the next sections.

### 3.1 Parameter estimation

We can use the analysis method presented in the last section to estimate the real space power spectrum and  $\beta$  maximizing the likelihood. Symbolically

$$\mathcal{L}(\beta, P) = \frac{1}{(2\pi)^{N/2} \|C\|^{1/2}} \exp\left(-\frac{1}{2} \sum_{\mu\nu} D_\mu C_{\mu\nu}^{-1} D_\nu\right). \quad (19)$$

where  $C$  is the covariance matrix of the  $N$  data values, dependent on the (parametrized)  $P(k)$  and  $\beta$ . Once again, the data are the real and imaginary parts of  $D_m(k)$ . The likelihood method has the advantage that all the aliasing ef-

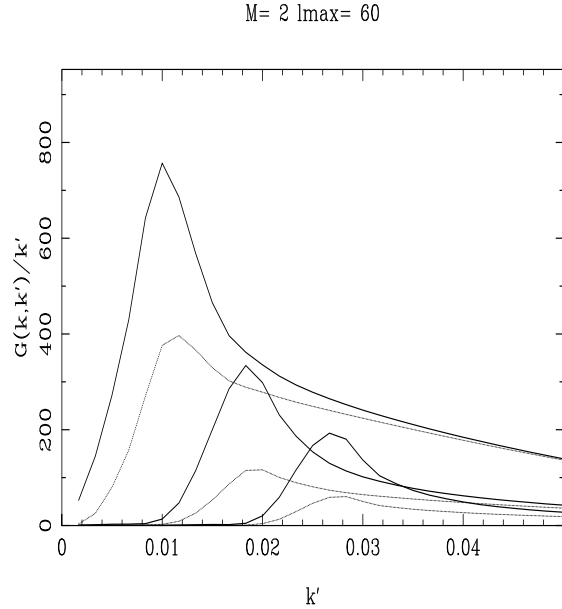


**Figure 2.** Kernel function for constant declination slice, for modes with  $m = 2$ , and, from left to right,  $k = 0.008, 0.016, 0.025h \text{ Mpc}^{-1}$ . Solid lines are for  $\beta = 1$ , dotted for  $\beta = 0$ .

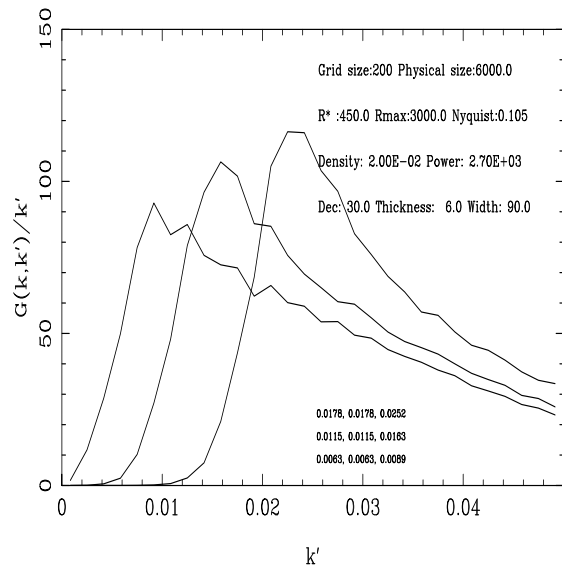


**Figure 3.** Kernel function for Fourier modes with same wavenumbers as Fig. 2.

fects are treated correctly, and we do recover 3D power estimates with correct error bars. We illustrate this method by analysing a numerical simulation created with Couchman's AP<sup>3</sup>M code (Couchman 1991). A slice between declinations 20 and 40 degrees is projected onto declination 30, with a right ascension range of 90 degrees. The power spectrum is a power-law  $P(k) \propto k^{-1}$ , and the likelihood for the amplitude of  $P(k)$  and  $\beta$  is shown in Figure 4. The details of the analysis are that the nonlinear wavenumber (where  $k^3 P(k)/(2\pi^2) = 1$ ) is 183 (units are arbitrary), and the analysis examines modes up to  $k_{\max} = 30$ . Pushing the maximum analysed wavenumber beyond this pushes  $\beta$  down, as the effects of Fingers-of-God become apparent. These could be reduced by including the effects of smoothing (cf. HT95), but they have not been incorporated here. The  $m$  modes are analysed in steps of 2 from 2 to 20, and the wavenumbers selected are from 6 to 30 in steps of 2. There is no difficulty in principle in taking every  $m$  and  $n$  mode, but there is a numerical problem as adjacent modes are too strongly correlated and the matrix becomes numerically singular. Note that modes separated by 2 are correlated, and the correlations correctly accounted for in (19). We also put a constraint on the wavenumber perpendicular to the line-of-sight, ensuring that it is not too nonlinear, by rejecting modes with  $m k/4.0 < k_{\max}$ . This ensures that the transverse wavenumber at the peak of  $j_2(kr)$  is no more than 4.0/3.3 times  $k_{\max}$ . Experimentation shows that this gives unbiased estimation of  $\beta$  and  $P(k)$ . The galaxies are weighted with the Feldman et al. (1994) optimized weighting  $w_s(r) = [1 + \rho_0(r)P(k)]^{-1}$  and  $P(k)$  in the weighting is taken as a constant, comparable to the true power in the simulation. The true parameters are shown by the encircled cross. We see that the method is capable of determining  $\beta$  and the power spectrum with somewhat larger errors than a fully 3D survey (HT95) with similar numbers of objects, and also note that here we need to examine larger wavelengths than in the 3D case (up to the nonlinear wavenumber/6, as opposed to nonlinear wavenumber/3 in the 3D case). Failure to do this leads to underestimation of  $\beta$  because of nonlinear effects.

### 3.2 Errors on $\beta$ and $P(k)$

In this section, we calculate the expected errors in a deep, thin-slice survey, such as might be achievable in the first year of the AAT 2dF survey. The error on the parameters is readily estimated using the Fisher information matrix (Tegmark, Taylor & Heavens 1996).

For a set of parameters  $\theta_i$ ,  $i = 1, N$  (e.g.  $\beta$  and the power spectrum in  $N - 1$  wavenumber bins), the covariance matrix of the parameter estimates is

$$\mathbf{T} = \langle \theta\theta^T \rangle - \langle \theta \rangle \langle \theta^T \rangle = \mathbf{F}^{-1} \quad (20)$$

where

$$F_{ij} \equiv \frac{1}{2} \text{Trace} (\mathbf{C}^{-1} \mathbf{C}_{,i} \mathbf{C}^{-1} \mathbf{C}_{,j}) \quad (21)$$

is the Fisher information matrix.  $\mathbf{C}$  is the covariance matrix of the data  $\langle \mathbf{D}\mathbf{D}^T \rangle$ , and  $\mathbf{C}_{,i} \equiv \partial \mathbf{C} / \partial \theta_i$ . The Fisher matrix is readily obtained from the data covariance matrix (16). To illustrate this, we calculate the parameter covariance matrix for a thin slice,  $6^\circ \times 90^\circ$ , with a Gaussian selection function  $\rho_0(r) = \rho_* \exp(-r^2/r_*^2)$ . We take  $\rho_* = 0.02h^3 \text{ Mpc}^{-3}$  and

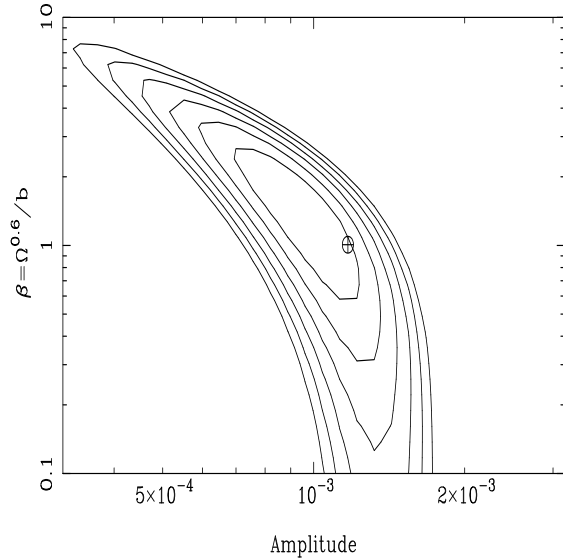


**Figure 4.** Likelihood function for the amplitude of the real-space power spectrum and  $\beta$  for a numerical simulation whose true parameters are shown by the cross. The contours are separated by 0.5 in  $\ln(\text{likelihood})$ .

$r_* = 450h^{-1} \text{ Mpc}$ , broadly comparable to an optical survey to a limit  $b = 19.5$  (cf forthcoming AAT and Sloan galaxy surveys).

We analyse modes from  $m = 2$  to  $m = 20$ , once again separated by 2 to avoid the covariance matrix becoming numerically singular. The  $k$  values are spaced by  $0.0167 h \text{ Mpc}^{-1}$ , and the modes are analyzed up to  $k = 0.05h \text{ Mpc}^{-1}$ , consistent with our previous numerical experiments for unbiased results. The summations extend to  $\ell = 60$ , and the  $k$  integrations extend to  $k = 0.165h \text{ Mpc}^{-1}$ . The galaxies are weighted with the Feldman et al. (1994) optimized weighting  $w_s(r) = [1 + \rho_0(r)P(k)]^{-1}$  and  $P(k)$  in the weighting is taken to be  $2700 h^{-3} \text{ Mpc}^3$ . The expected error on  $\beta$  from such a slice is 0.236, and the expected fractional error in the power is shown in Fig. 5, for a power spectrum assumed to be smooth on a scale of  $0.0167 h \text{ Mpc}^{-1}$ . Increasing the width of these  $k$  bins decreases the error. Note how the error increases at the high- $k$  end beyond the maximum wavenumber analysed ( $4.0/3.3$  times  $0.05 h \text{ Mpc}^{-1} \simeq 0.06$ ), and at the low-end, where the size of the survey becomes comparable to the wavelength ( $2\pi/r_* \simeq 0.014$ ). The correlation matrix for the parameters is shown in Table 1. This analysis takes only a matter of minutes on a workstation, once the matrices  $\Phi$  and  $V$  have been calculated. These take a few hours, but are calculated once only for a given survey. What is apparent from this example is that, even for a deep survey with many objects,  $P(k)$  is detected on scales of the survey  $k \sim 2\pi/450 \sim 0.014h \text{ Mpc}^{-1}$ , but not with good accuracy.  $\beta$  estimation is actually not bad (error 24%), but this could be improved noticeably (to 15%) if the 3D power spectrum is determined independently, from a sky-projected

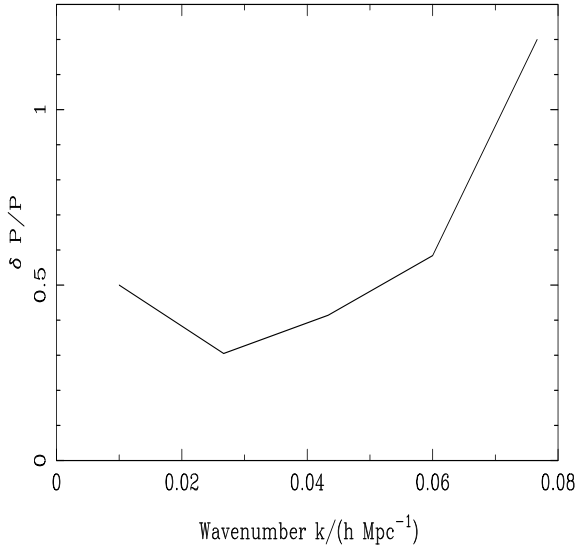


**Figure 5.** Expected fractional error on  $P(k)$  from a deep thin slice survey, for narrow bins in  $k$ -space. For details, see text.

catalogue such as the APM survey. An application of this method to the Las Campanas survey (Shectman et al. 1995) is in progress.

$\beta$	$P_1$	$P_2$	$P_3$	$P_4$	$P_5$
1.00	-0.36	-0.29	-0.43	-0.21	0.10
-0.36	1.00	-0.21	0.21	0.03	-0.04
-0.29	-0.21	1.00	-0.24	0.12	-0.03
-0.43	0.21	-0.24	1.00	-0.12	-0.24
-0.21	0.03	0.12	-0.12	1.00	-0.58
0.10	-0.04	-0.03	-0.24	-0.58	1.00

**Table 1.** Correlation matrix for the parameters, in the order  $\beta$  and the five fractional power spectrum measurements in order of increasing  $k$ .

#### 4 3D SURVEYS: OPTIMIZING FOR POWER ESTIMATION

We have shown in the previous section how the expected error on a parameter may be estimated in advance for a given analysis method and survey design. The conclusion that 2D surveys are not particularly good for determining large-scale 3D power suggests that genuine 3D surveys may be more profitable. The issues of design and analysis are also relevant in 3D, and here we consider the problem of optimising the design of a galaxy redshift survey to measure the power spectrum on some particular scale. The typical decisions to be made are whether to go for a deep survey over

a small area of sky, or a shallower survey over a wider area of sky. We also consider whether it makes sense to sparse-sample the galaxies, or to observe every one. This section is essentially a Fourier analogue of Kaiser’s (1986) treatment of sparse-sampling to estimate the two-point correlation function, generalized to account for a radial selection function, and with the proper power error estimate of Feldman, Kaiser & Peacock (1994) incorporated.

For simplicity, we make the following assumptions: we assume that the effects of redshift-space distortions are small, and we assume that the observing time for each galaxy is proportional to the inverse square of its flux. The former is motivated by earlier studies (HT95) where the optimal weighting was found to be insensitive to the degree of redshift distortion (see also Hamilton 1996). The latter assumption is an example; different constraints, for fibre systems for example, could be incorporated if desired. Our prime constraint is that the total duration of observing is taken to be fixed. In considering sparse-sampling, we restrict attention to a sparse-sample fraction which is constant for all galaxies in the parent sample. Thus, for example, we do not consider a variable sparse-sampling rate which depends on flux.

It was shown by Feldman et al. (1994), HT95 and Hamilton (1996) that the optimal weighting of galaxies in the survey is

$$w(\mathbf{r}) = \frac{1}{1 + f\bar{n}(\mathbf{r})P(k)} \quad (22)$$

where  $P(k)$  is the (prior estimate of) the power to be measured, and  $\bar{n}(\mathbf{r})$  is the mean number density of galaxies at position  $\mathbf{r}$ . We introduce the possibility of sparse-sampling by multiplying this number density by a factor  $f$ .

Feldman et al. demonstrated that this weighting gives rise to an error in the power of  $\sigma_P^2/P^2 = (2\pi)^3/(V_{\mathbf{k}}I)$ , where  $V_{\mathbf{k}}$  is the volume of  $k$ -space over which the power is averaged, and

$$I(f, S, \Omega) = \Omega \int dr \frac{r^2}{\left(1 + \frac{1}{fP\bar{n}(r)}\right)^2}. \quad (23)$$

Here  $S$  and  $\Omega$  are the flux limit and solid angle of the survey. Our problem then reduces to maximising  $I$  with respect to  $f$ ,  $S$  and  $\Omega$ , subject to the constraint that the total observing time is fixed.

To do this optimisation, we need the luminosity function  $\Phi(L)$ , from which the number density is obtained:

$$\bar{n}(r, S) = n_0(X) \equiv \int_X^\infty dL \Phi(L). \quad (24)$$

where  $X = 4\pi r^2 S$ . If the time to observe an object of flux density  $S'$  is  $\lambda/(16\pi^2 S'^2)$  for some constant  $\lambda$ , then the time to observe a fraction  $f$  of all objects to a flux limit  $S$  in a solid angle  $\Omega$  reduces to

$$\begin{aligned} t(f, S, \Omega) &= \Omega f \int_0^\infty dr \lambda r^6 \int_{4\pi r^2 S}^\infty dL \frac{\Phi(L)}{L^2} \\ &= \frac{\Omega \lambda f}{2(4\pi S)^{7/2}} \int_0^\infty dX X^{5/2} n_2(X) \end{aligned} \quad (25)$$

where  $n_2(X) \equiv \int_X^\infty dL \Phi(L) L^{-2}$ .

The time constraint then simply yields  $S \propto (\Omega f)^{2/7}$ , and the error is minimised when

$$\frac{\Omega^{4/7}}{f^{3/7}} \int dX \frac{X^{1/2}}{\left(1 + \frac{1}{f P n_0(X)}\right)^2} \quad (26)$$

is maximised.  $\Omega$  and  $f$  may be chosen freely, apart from the obvious limits, with the depth of the survey  $S$  being dependent on the choice. We see immediately that the error is minimised if  $\Omega$  is made as large as possible. This is a quite general result, consistent with the general knowledge that surveys should be wide before being deep. If we fix the solid angle of the survey (as large as convenient), then we can straightforwardly solve for  $f$  to optimize the error. The analysis is readily generalized for observing times which are proportional to  $S^{1-\alpha} r^{-\beta}$  ( $\alpha = \beta = 2$  might be appropriate for fixed-width slit spectroscopy). In this case, one maximizes

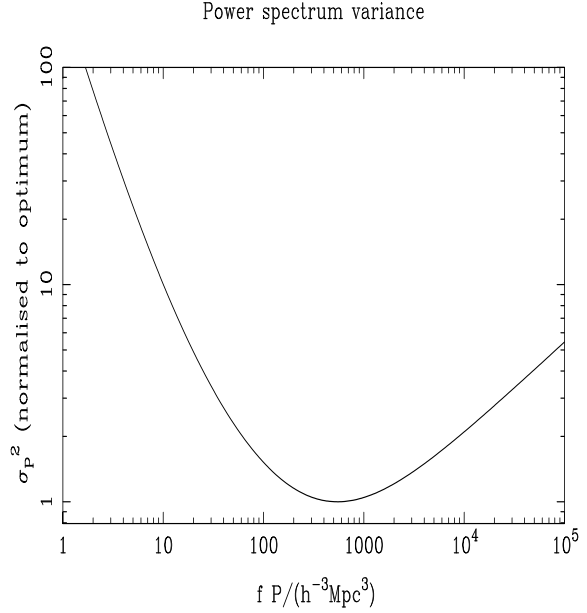
$$f^{-\frac{1}{1+2\alpha/3-\beta/3}} \int dX \frac{X^{1/2}}{\left(1 + \frac{1}{f P n_0(X)}\right)^2}. \quad (27)$$

Fig. 6 illustrates the effect for a Schechter luminosity function  $\Phi(L)dL = \phi^*(L/L^*)^{-1.3} \exp(-L/L^*)dL/L^*$ , with  $\phi^* = 0.013h^3 \text{ Mpc}^{-3}$ . The optimal sampling occurs at  $fP \simeq 500h^{-3} \text{ Mpc}^3$ , although of course  $f$  itself is bounded above by unity. To the left of the minimum, shot noise becomes dominant, whereas to the right, the extra sampling reduces the volume observable, so that cosmic variance dominates. To estimate  $f$ , the power at a wavenumber  $k = 0.01$  to  $0.1h \text{ Mpc}^{-1}$  is about  $1000\text{--}10000 h^{-3} \text{ Mpc}^3$ , depending on the galaxy type and theoretical prejudice (e.g. Baugh & Efstathiou 1993,1994, Ballinger et al. 1995), which motivates a sparse-sampling strategy of  $f \simeq 0.1$ . The error rises rapidly if  $fP \lesssim 100$ , so one must take care not to under-sample. If the power spectrum on large scales has the Zel'dovich form  $P \propto k$ , a survey to measure very large-scale power should be sampled fully.

## 5 CONCLUSIONS

In this paper we have presented a new method for analysing thin, near-constant declination slice surveys, using a 2D projection and expansion in radial and angular functions. We have also considered the optimisation problem of depth and sparse-sampling for 3D surveys. There are two main advantages of using spherical coordinates for analysis. The first is that the survey is usually defined by a fixed areal coverage, and a flux limit which leads to a selection function which is purely radial. The second advantage is that the effect of redshift distortion is radial, so it is straightforward to include it in the analysis. By expanding in spherical and angular functions, one can treat linear redshift distortions without further approximations, and this allows, in particular, analysis of long-wavelength modes which do not subtend small angles on the sky. By using carefully chosen radial functions for the analysis, one can ensure that the modes one analyses essentially include only 3D modes which are still linear.

For an all-sky survey, the formalism leads to very simple analysis, and this method is clearly the best we have to date. What was not clear was whether the method could be adapted for surveys of relatively small areal coverage,



**Figure 6.** The unnormalised variance in the power spectrum for a fixed solid angle and a Schechter luminosity function, as a function of the sparse-sample fraction  $f$  and the power spectrum to be estimated. The details of the luminosity function are given in the text, and the units of  $P$  are  $h^{-3} \text{ Mpc}^3$ .

since the mixing of modes of different  $\ell$  and  $m$  make the expansion more cumbersome. This paper shows that, even with this, essentially 2D surveys, one can retain the advantages of the spherical expansion without severe additional complexity. Our error analysis shows that 3D power can be estimated from 2D surveys, properly including the effects of aliasing, mode-mode correlations, shot noise and cosmic variance. However, the reduction in dimensionality means the errors achievable are unlikely to be very small. This is in contrast to 3D surveys, where small errors on the real-space power spectrum can be achieved from the Fourier-Bessel technique (Ballinger, Heavens & Taylor 1995). In 2D,  $\beta$  can be determined with reasonable accuracy (about 25%), but the best approach will probably be to use a sky-projected catalogue to estimate the 3D power independently, and then to use spherical harmonics with the slice to measure  $\beta$  with higher accuracy (about 15%).

We also show in this paper that 3D surveys may be optimised for measuring 3D power, given a constraint on total observing time, by choosing as wide an area of sky as possible, and by sparse-sampling at a rate which is dependent on the expected power to be measured.

## APPENDIX

In this appendix, we calculate the covariance matrix for the continuous spherical transform. We transform the density field  $\delta(\mathbf{r}) = \frac{1}{(2\pi)^3} \int d^3\mathbf{k} \delta_{\mathbf{k}} e^{i\mathbf{k}\cdot\mathbf{r}}$  and expand the exponential

as a sum of Bessel functions

$$\delta(\mathbf{r}) = \frac{1}{2\pi^2} \int dk d\Omega_{\mathbf{k}} \delta_{\mathbf{k}} \times \sum_{\ell m} i^\ell j_\ell(kr) Y_\ell^m(\theta_{\mathbf{k}}, \varphi_{\mathbf{k}}) Y_\ell^m(\theta, \varphi) k^2 \quad (28)$$

where  $\Omega_{\mathbf{k}} = (\theta_{\mathbf{k}}, \varphi_{\mathbf{k}})$  is the direction of the  $\mathbf{k}$  vector, and  $(\theta, \varphi)$  is the direction of  $\mathbf{r}$ . The definition of the spherical harmonics used in this paper is that found in Binney & Tremaine (1987):

$$Y_\ell^m(\theta, \phi) = \sqrt{\frac{2\ell+1}{4\pi} \frac{(\ell-|m|)!}{(\ell+|m|)!}} P_\ell^{|m|}(\cos\theta) \times \exp(im\phi) \times \begin{cases} (-1)^m & m \geq 0 \\ 1 & m < 0 \end{cases} \quad (29)$$

The spherical expansion is

$$\delta_{\ell m}(k) = \sqrt{\frac{2}{\pi}} \int \delta(\mathbf{r}) j_\ell(kr) Y_\ell^m(\theta, \varphi) d^3\mathbf{r} \quad (30)$$

which becomes

$$\delta_{\ell m}(k) = (2\pi)^{-3/2} i^\ell \int d\bar{k} d\Omega_{\bar{\mathbf{k}}} \delta_{\bar{\mathbf{k}}} Y_\ell^m(\theta_{\bar{\mathbf{k}}}, \varphi_{\bar{\mathbf{k}}}) \delta^D(k - \bar{k}) \quad (31)$$

where we have used the orthogonality (Binney & Quinn 1991)

$$\int d\Omega dr j_{\ell'}(k'r) j_\ell(kr) r^2 Y_{\ell'}^{m'*}(\theta, \varphi) Y_\ell^m(\theta, \varphi) = \frac{\pi}{2kk'} \delta^D(k - k') \delta_{\ell\ell'}^K \delta_{mm'}^K \quad (32)$$

where  $\delta^D$  and  $\delta^K$  are Dirac and Kronecker delta functions respectively. The covariance matrix is

$$\langle \delta_{\ell m}(k) \delta_{\ell' m'}^*(k') \rangle = (2\pi)^{-3} i^{\ell-\ell'} \int d\bar{k} d\bar{k}' d\Omega_{\bar{\mathbf{k}}} d\Omega_{\bar{\mathbf{k}}}' \langle \delta_{\bar{\mathbf{k}}} \delta_{\bar{\mathbf{k}}}'^* \rangle Y_\ell^{m*}(\theta_{\bar{\mathbf{k}}}, \varphi_{\bar{\mathbf{k}}}) Y_{\ell'}^{m'}(\theta_{\bar{\mathbf{k}}}', \varphi_{\bar{\mathbf{k}}}') \delta^D(k - \bar{k}) \delta^D(k' - \bar{k}') \quad (33)$$

Defining the power spectrum by

$$\langle \delta_{\bar{\mathbf{k}}} \delta_{\bar{\mathbf{k}}}'^* \rangle = (2\pi)^3 P(\bar{k}) \delta^D(\bar{\mathbf{k}} - \bar{\mathbf{k}}') \\ = (2\pi)^3 P(\bar{k}) \frac{\delta^D(\bar{k} - \bar{k}')}{\bar{k}^2} \delta^D(\mu_{\bar{\mathbf{k}}} - \mu_{\bar{\mathbf{k}}}') \delta^D(\varphi_{\bar{\mathbf{k}}} - \varphi_{\bar{\mathbf{k}}}') \quad (34)$$

( $\mu \equiv \cos\theta$ ) the analogous expression of orthogonality for the Fourier-Bessel modes is

$$\langle \delta_{\ell m}(k) \delta_{\ell' m'}^*(k') \rangle = P(k) \frac{\delta^D(k - k')}{k^2} \delta_{\ell\ell'}^K \delta_{mm'}^K \quad (35)$$

The power is evenly divided between real and imaginary parts, except for  $m = 0$  modes, which are real.

### Redshift distortions

In a redshift space map, galaxies are placed at a position  $\mathbf{s} = (s, \theta, \phi)$ , where the distance coordinate  $s$  is the recession velocity divided by the Hubble constant  $H_0$ . In general this is not the true distance because the galaxy may have a peculiar velocity  $\mathbf{v}$ . The redshift space position is then related to the real-space position  $\mathbf{r}$  by

$$\mathbf{s}(\mathbf{r}) = \mathbf{r} \left[ 1 + \frac{(\mathbf{v} - \mathbf{v}_0) \cdot \mathbf{r}}{H_0 r^2} \right] \quad (36)$$

where  $\mathbf{v}_0$  is the peculiar velocity locally.

To expand the spherical expansion to linear order, we first note that  $\rho(\mathbf{r}) d^3\mathbf{r} = \rho(\mathbf{s}) d^3\mathbf{s}$ , and make a Taylor expansion of the resulting integrand to first order in  $s - r$

$$j_\ell(ks) w_s(s) \simeq j_\ell(kr) w_s(r) + (s - r) \frac{d}{dr} [j_\ell(kr) w_s(r)]. \quad (37)$$

To obtain an expression for  $s - r$ , we assume potential flow  $\mathbf{v} = -\nabla\Phi$  (valid for linear, growing-mode perturbations), where  $\Phi(\mathbf{r})$  is the velocity potential. The effect of the local group velocity  $\mathbf{v}_0$  is to add an extra term to the mean of the transform coefficients, and will be treated separately. Expanding  $\Phi$  in terms of  $\Phi_{\ell m}(k)$ , we find

$$s - r = \frac{\mathbf{v} \cdot \hat{\mathbf{r}}}{H_0} \\ = -\frac{1}{H_0} \sqrt{\frac{2}{\pi}} \sum_{\ell m} \int dk \Phi_{\ell m}(k) \frac{dj_\ell(kr)}{dr} Y_\ell^{m*}(\theta, \varphi) k^2. \quad (38)$$

The peculiar Poisson equation  $\nabla^2\Phi = \beta\delta(\mathbf{r})$  relates the potential to the galaxy overdensity field, which leads to  $\Phi_{\ell m}(k) = -\beta\delta_{\ell m}(k)/k^2$ . From this we find (choosing units such that  $H_0 = 1$ )

$$s - r = \beta \sqrt{\frac{2}{\pi}} \sum_{\ell m} \int dk \delta_{\ell m}(k) \frac{dj_\ell(kr)}{dr} Y_\ell^{m*}(\theta, \varphi). \quad (39)$$

This leads to the  $V$  matrix terms in the main text. The effect of the local group velocity is to add the following to the mean value of  $D_m(k)$ :

$$\frac{v_0}{H_0} \sqrt{\frac{2}{\pi}} \int dr \left( r^2 \frac{d\rho_0}{dr} + 2r\rho_0 \right) w_s(r) f(kr) \\ \int d\Omega w_\Omega(\Omega) \exp(-im\varphi) \hat{\mathbf{v}}_0 \cdot \hat{\mathbf{r}} \quad (40)$$

where  $\hat{\mathbf{r}}$  and  $\hat{\mathbf{v}}_0$  are unit vectors.

## REFERENCES

- Ballinger W.E., Heavens A.F., Taylor A.N., 1995, MNRAS, 276, L59  
 Baugh C.M., Efstathiou G.P., 1993, MNRAS, 265, 145  
 Baugh C.M., Efstathiou G.P., 1994, MNRAS, 267, 323  
 Binney J., Quinn T., 1991, MNRAS, 249, 678  
 Binney J., Tremaine S., 1987, Galactic Dynamics, Princeton University Press, Princeton  
 Broadhurst T.J., Ellis R.S., Koo D.C., Szalay A.S., 1990, Nat, 343, 726  
 Cole S., Fisher K., Weinberg D., 1994, MNRAS, 267, 785  
 Couchman H.M.P., 1991, ApJ, 368, 23  
 Fabbri R., Natale V. 1990, ApJ, 363, 3  
 Feldman H.A., Kaiser N., Peacock J.A., 1994, ApJ, 426, 23  
 Fisher K.B., Scharf C.A., Lahav O., 1994a, MNRAS, 266, 219  
 Fisher K.B., Davis M., Strauss M.A., Yahil A., Huchra J.P., 1994b, MNRAS, 267, 927  
 Fisher K.B., Lahav O., Hoffman Y., Lynden-Bell D., Zaroubi S., 1995, MNRAS, 272, 885

- Hamilton A., 1992, *ApJ*, 385, L5  
Hamilton A., 1996, *MNRAS*, in press  
Heavens A.F., Taylor, A.N., 1995, *MNRAS*, 275, 483  
Kaiser N., 1986, *MNRAS*, 219, 785  
Kaiser N., 1987, *MNRAS*, 227, 1  
Kaiser N., Peacock J.A., 1991, *ApJ*, 379, 482  
Landy S.D., Shectman S.A., Lin H., Kirshner R.P., Oemler A.A., Tucker D., 1996, *ApJ*, 456, L1  
Lahav O., 1993, in *Proc. 9th IAP Conference, Cosmic Velocity Fields*, ed. Bouchet, F., Lachiéze-Rey, M., Editions-Frontières, Gif-Sur-Yvette  
Scharf C.A., Hoffman Y., Lahav O., Lynden-Bell D., 1992, *MNRAS*, 259, 229  
Scharf C.A., Lahav O., 1993, *MNRAS*, 264, 439  
Shectman S.A., Landy S.D., Oemler A., Tucker D.L., Kirshner R.P., Lin H., Schechter P.L., 1995, in *Wide-Field Spectroscopy and the Distant Universe, Proc 35th Herstmonceux Conference*, ed. Maddox S.J., Aragon-Salamanca A. (Singapore, World Scientific), 98  
Zaroubi S., Hoffman Y., 1996, *ApJ*, 462, 25